SPHERE IRDIS and IFS astrometric strategy and calibration

Anne-Lise Maire[a], Maud Langlois[b,c], Anne-Marie Lagrange[d], Raffaele Gratton[e], Gaël Chauvin[d], Silvano Desidera[e], Julien H. Girard[f,d], Arthur Vigan[c], Philippe Delorme[d], Jean-Luc Beuzit[d], Riccardo U. Claudi[e], Kjetil Dohlen[c], Markus Feldt[a], David Mouillet[d], Pascal Puget[d], Massimo Turatto[e], François Wildi[g]

[a]Max Planck Institute for Astronomy, Königstuhl 17, 69117 Heidelberg, Germany
[b]CRAL, Univ. Lyon 1, ENS Lyon, CNRS, 9 av. Ch. André, 69561 Saint-Genis-Laval, France
[c]LAM, Aix Marseille Univ., CNRS, B.P. 8, 13376 Marseille, France
[d]IPAG, Univ. Grenoble Alpes, CNRS, B.P. 53, 38041 Grenoble, France
[e]INAF, Astronomical Observatory of Padova, Vicolo dell'Osservatorio 5, 35122 Padova, Italy
[f]ESO, Alonso de Cordova 3107, Casilla 19001 Vitacura, Santiago 19, Chile
[g]Geneva Observatory, Univ. of Geneva, Chemin des Maillettes 51, 1290 Versoix, Switzerland

ABSTRACT

We present the current results of the astrometric characterization of the VLT planet finder SPHERE over 2 years of on-sky operations. We first describe the criteria for the selection of the astrometric fields used for calibrating the science data: binaries, multiple systems, and stellar clusters. The analysis includes measurements of the pixel scale and the position angle with respect to the North for both near-infrared subsystems, the camera IRDIS and the integral field spectrometer IFS, as well as the distortion for the IRDIS camera. The IRDIS distortion is shown to be dominated by an anamorphism of 0.60±0.02% between the horizontal and vertical directions of the detector, i.e. 6 mas at 1 arcsec. The anamorphism is produced by the cylindrical mirrors in the common path structure hence common to all three SPHERE science subsystems (IRDIS, IFS, and ZIMPOL), except for the relative orientation of their field of view. The current estimates of the pixel scale and North angle for IRDIS are 12.255±0.009 milliarcseconds/pixel for H2 coronagraphic images and -1.70±0.08°. Analyses of the IFS data indicate a pixel scale of 7.46±0.02 milliarcseconds/pixel and a North angle of -102.18±0.13°. We finally discuss plans for providing astrometric calibration to the SPHERE users outside the instrument consortium.

Keywords: extrasolar planets, high-contrast imaging, astrometry, distortion, integral field spectroscopy

1. INTRODUCTION

The detection and characterization of exoplanets is one of the most active research areas in modern astrophysics. Many methods are employed to address specific types of objects and/or questions. High-contrast imaging is currently the most efficient technique for probing (1) the architecture of systems with wide-separated (beyond ∼5–10 AU) Jovian mass planets and (2) the spectral properties of these planets[1–3]. A key science motivation for these studies is to understand whether this population of planets is the large-separation tail of the distribution of planets discovered by radial velocity and transit surveys at shorter separations or they form a separated planet population with different formation mechanisms. Astrometry is critical to confirm the companionship of detected companion candidates from the comparison of the measured relative position at two separated epochs to the predicted positions under the hypothesis that they are background objects. For short-period systems, accurate astrometric monitoring is needed to constrain the orbital elements of the individual companions (e.g., period, semi-major axis, eccentricity, inclination) and the total dynamical mass hence provides insights into the dynamical properties (e.g., mean motion resonances, dynamical interactions, orbital stability). The orbital elements can be compared to predictions from different formation scenarios for substellar companions (core accretion, gravitational instability in a circumstellar disk, collapse and fragmentation of a molecular cloud) to constrain the formation mechanisms of the systems[4,5]. If radial velocity measurements or astrometric motion of the central star are available, the dynamical mass of the companions can be constrained[6–8]. Dynamical

---

mass measurements provide critical tests for atmospheric and evolutionary models for brown dwarfs and giant planets[9–12]. Most of the young directly-imaged substellar companions have semi-major axis larger than a few tens of AU, so that estimates for their mass can only be inferred from their luminosity assuming possible ranges for the system age and evolutionary models. However, these estimates are strongly uncertain because the models are poorly calibrated at young ages and low masses. Detecting and measuring the orbit of young and low-mass substellar companions provide valuable benchmarks for the models.

The detection and the orbital analysis of young and low-mass substellar companions are a major part of the science case for the recently commissioned planet finder SPHERE[13] (Spectro-Polarimetric Exoplanet REsearch). The instrument includes an extreme adaptive optics system[14], with a pupil stabilization control system and stress polished toric mirrors[15] to relay the beam to the coronagraphs[16] and the science instruments. The science instruments are composed of the infrared dual-band imager and spectrograph IRDIS[17], the near-infrared integral field spectrometer IFS[18], and the rapid-switching visible imaging polarimeter ZIMPOL[19]. SPHERE has been successfully commissioned at the Very Large Telescope from May to October 2014 and is offered to the community since April 2015. The SPHERE consortium guaranteed-time survey consists of 260 nights over 5 years, from which 200 nights are dedicated to a large census in the near-infrared of the population of young giant planets and brown dwarfs at wide orbits ($\gtrsim$5 AU). The main observing mode used for this survey consists in simultaneous observations in the YJ bands (0.95–1.35 μm, $R \sim 54$) with IFS (field of view $1.73'' \times 1.73''$) and in the H-band ($H_2 = 1.593$ μm and $H_3 = 1.667$ μm) with IRDIS (field of view $11'' \times 12.5''$) in dual-band imaging mode[20]. A coronagraphic mask common to both instruments is used to attenuate the stellar light[16]. Both IRDIS and IFS are operated in pupil-stabilized mode to take advantage of the angular differential imaging technique[21] to further suppress the stellar residuals in the images. High-precision relative astrometry and efficient attenuation of the stellar residuals by image post-processing techniques critically depend of a precise estimate of the location of the star behind a coronagraphic mask[22, 23]. For this purpose, a calibration image is recorded before and after a science sequence with four crosswise faint stellar replicas produced by applying a periodic modulation on the SPHERE deformable mirror[24]. The specifications for the SPHERE astrometric accuracy are 5 mas (goal 1 mas). Extensive tests using injections of synthetic point sources in laboratory data processed with spectral differential imaging[25, 26] resulted in astrometric accuracies below 1.5–2 mas for detections at signal-to-noise ratios above 10[27].

We present in this paper the current on-sky status and results of the astrometric characterization of IRDIS and IFS based on 2 years of SPHERE operations from 2014 to 2016. We describe in Sec. 2 our criteria for the selection of the astrometric fields. We present in Sec. 3 the on-sky measurements of the SPHERE optical distortion, the zeropoint angle of the SPHERE pupil in pupil-stabilized mode, and the pixel scale and true North offset for both IRDIS and IFS. We summarize our main results and briefly discuss a few prospects in Sec. 4.

2. METHODOLOGY

2.1 Strategy for the SPHERE astrometric characterization

In the case of the SPHERE planet-search observations, five parameters need to be estimated: the IRDIS pixel scale and true North offset, the IFS pixel scale and its relative orientation with respect to IRDIS, and the zeropoint angle of the SPHERE pupil in pupil-stabilized mode. The pixel scale of IRDIS is slightly dependent on the selected filter, while both IRDIS and IFS pixel scales depend on the use or not of a coronagraph because of the coronagraphic glass plate located at the focal plane. The true North offset shall be monitored regularly with time since it is expected to exhibit small variations ($<1°$), especially after technical interventions on the instrument. The zeropoint angle of the instrument pupil in pupil-stabilized mode is expected to be affected by systematics due to the limited accuracy of the derotator positioning.

For the estimation of the pixel scales and the IRDIS true North offset, an absolute weekly calibration is needed using astrometric fields with accurate positions (including, if possible, the stellar proper motions). Stellar clusters are suitable targets for this purpose as they can provide several tens of stars for the analysis. Stellar cluster fields can also be used to derive the SPHERE+VLT optical distortion, although the optical distortion of the VLT is expected to be small (on-sky measurements of the Galactic Center with NaCo indicated distortion effects below 0.1 mas over a $5.4''$ field of view[28]). Another advantage of this method over the use of internal distortion grids

for measuring the SPHERE distortion is that it does not rely on a model for the reference grid. The zeropoint angles for IFS and the SPHERE pupil in pupil-stabilized mode are relative parameters, so even an astrometric binary with large uncertainties on its orbital properties is suitable for their estimation.

2.2 SELECTION OF THE CALIBRATION FIELDS

The selection of the calibration fields was done considering the following criteria:

- the type of parameters to be estimated (absolute/relative);

- the availability of accurate reference positions from HST measurements;

- the presence of a bright star for AO guiding ($R \lesssim 13.5$ mag);

- for binaries, an H-band magnitude for the components fainter than 8.6 mag to avoid the use of neutral density filters to get unsaturated images at the shortest integration times (0.83 s for IRDIS, 1.66 s for IFS);

- the use of the field for previous astrometric monitorings*;

- a good on-sky coverage throughout the year.

We selected as main observing fields 47 Tucanae, the Orion Trapezium B1–B4, NGC 3603, and NGC 6380 (Tab. 1 and Fig. 1), plus a handful of long-period binaries (HIP 67745, HIP 68725, HIP 102979) with Hipparcos data and separations greater than the IFS field of view (separations ∼2–5″). The catalogs of the stellar positions for these fields come from various sources: Washington Double Star (WDS) catalog† for the binaries, literature for the Orion Trapezium B1–B4[29], and private requests for 47 Tucanae (A. Bellini/STScI), NGC 6380 (E. Noyola/Univ. Texas Austin), and NGC 3603[30] (Z. Khorrami/OCA).

For the binaries, we fitted linear equations to the WDS data with increased weights on the Hipparcos data for predicting their relative position with their uncertainty at the epoch of the SPHERE observations. However, the discrepancies between the measured and expected separations and position angles are usually larger than the fitting uncertainties. When a stellar cluster field was observed close in time to a binary, we recalibrated the predicted position to the position derived using the astrometric calibration provided by the stellar cluster. The upcoming release of the first GAIA data in autumn 2016 will finally allow a full determination of the absolute positions of several of our astrometric standards, allowing in the future a more accurate absolute astrometric calibration of the SPHERE data.

When observing the Orion Trapezium B1–B4, NGC 3603 and the binaries with a coronagraph, the AO guide star is offsetted out of the coronagraphic mask using a tip-tilt mirror so that it can be used for the astrometry. Most astrometric data were recorded in field-stabilized mode.

Table 1. Coordinates of the AO guide star for the stellar clusters used as references for the SPHERE astrometric fields.

Field	47 Tucanae	NGC 3603	NGC 6380
RA (J2000)	00:23:58.12	11:15:07.48	17:34:28.11
DEC (J2000)	-72:05:30.19	-61:15:38.70	-39:04:50.56

We selected 47 Tucanae as reference astrometric field for the recalibration of the other SPHERE astrometric fields because of the availability of the individual stellar proper motions in the HST catalog (accuracy 0.3 mas/yr, reference epoch 2006.20, see [31] for the methods used for their derivation).

---

*It has not been possible to use NaCo observations for the astrometric calibration of SPHERE until December 2015 because NaCo was removed from the VLT in September 2013 for technical interventions. After a recommissioning on another VLT telescope in January 2015, it was again removed in March 2015 because of technical issues and was unavailable until December 2015.
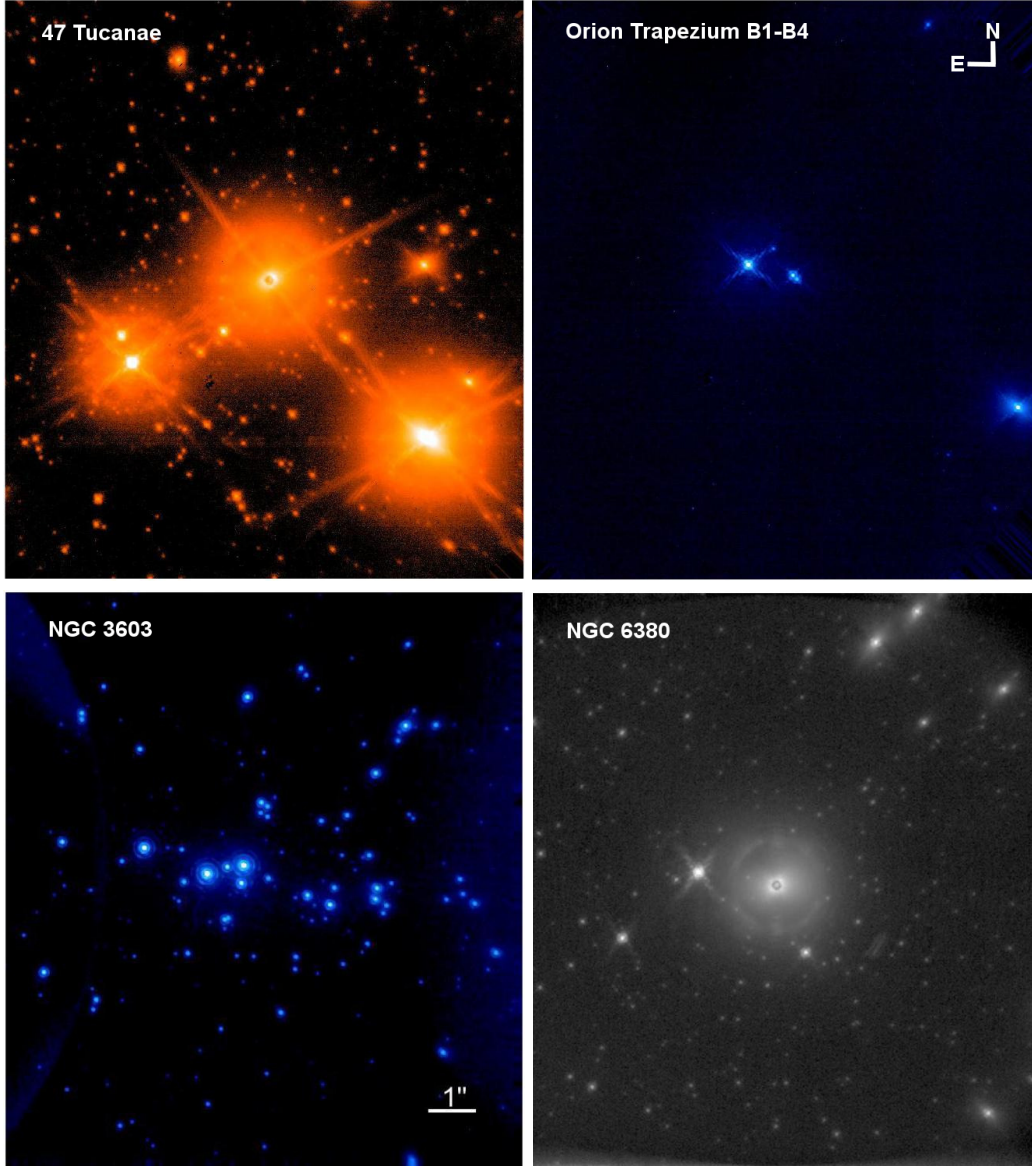
†http://www.usno.navy.mil/USNO/astrometry/optical-IR-prod/wds/WDS/.

Figure 1. IRDIS images of the main reference SPHERE astrometric fields.

3. ASTROMETRIC RESULTS FROM JULY 2014 TO MAY 2016

All data were reduced with the SPHERE data reduction pipeline[32] and analyzed with custom IDL routines to derive the astrometric calibration. For data obtained in field-stabilized mode, the individual frames are first selected based on the flux statistics and combined to enhance the signal-to-noise ratio of the detected stars. Then, the positions of the stars are measured with Gaussian fitting using the mpfit library[33]. The counter-identification between the SPHERE positions and the catalog positions is done using estimates for the separations and the position angles assuming approximate values for the SPHERE pixel scale and true North offset (plus the IFS angle offset relative to IRDIS for IFS observations) and tolerance criteria. After the counter-identification, the average pixel scale and true North offset are derived from the statistics of all the available stellar pairs after removing outliers using sigma clipping. If several tens of stars are available, the SPHERE positions are corrected for the on-sky optical distortion (Sec. 3.1) before deriving the astrometric calibration. The on-sky optical distortion is measured by fitting linear coordinate transformations between the catalog and the SPHERE positions. If few
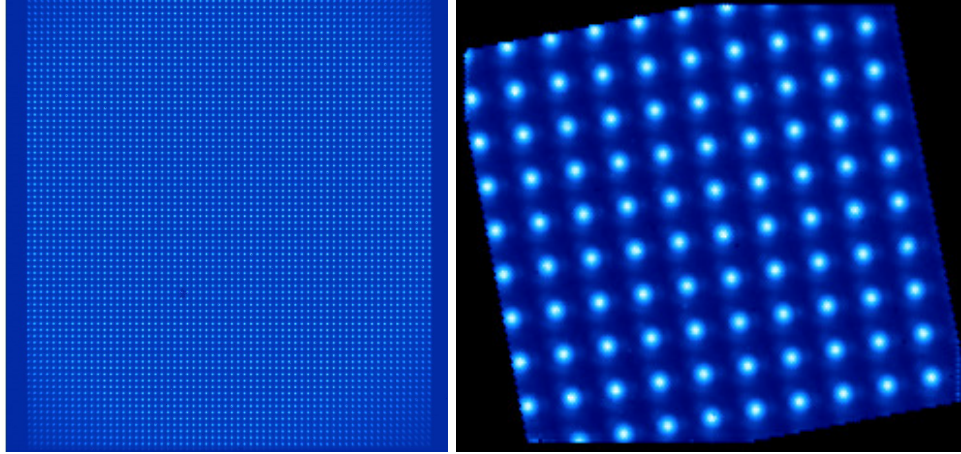
Figure 2. Left-side IRDIS image (left) and combined IFS image (right) of the illuminated SPHERE pinhole grid (spacing 100.0±0.5 µm). The numbers of visible pinholes differ due to different sizes of the IRDIS and IFS fields of view.

stars are detected in the field, a default distortion correction is applied instead. In the case of pupil-stabilized data, the whole procedure is similar, except that the individual frames are corrected for the SPHERE distortion and derotated with respect to the first frame in the sequence prior to their combination. In this case, the estimated angle offset is the sum of the true North and the SPHERE pupil angle offsets. All angles provided in the following sections are counted positive from North to East. Work is on-going for implementing generic astrometric calibration values in the SPHERE data reduction pipeline. For now, proper astrometric calibration of the consortium guaranteed-time data is accounted for in custom IDL routines implemented in the SPHERE Data Center (IPAG/CNRS).

3.1 SPHERE OPTICAL DISTORTION

The strategy for the measurement of the instrument optical distortion is to use (1) crowded stellar cluster fields for the absolute calibration of one instrument setup (filter pair, coronagraph) and (2) data of internal distortion grids for differential correction between different instrument setups.

A square grid of transparent dots engraved in a layer of black chrome is located in the calibration unit of SPHERE[34] hence is common to all SPHERE science subsystems (Fig. 2). The pitch of the grid is 100.0±0.5 µm for a size of the dots of 30 µm.

Laboratory measurements showed that the cylindrical mirrors in the SPHERE common path are the main source for the instrument optical distortion, hence these distortion effects are common to IRDIS and IFS. For IFS, the distortion pattern is rotated by $+100.48\pm0.10°$, the position angle of the IFS field of view with respect to the IRDIS field of view (Sec. 3.4). The distortion pattern is not affected by the stabilization mode of SPHERE (stabilization of the instrument pupil or of the on-sky field) since the instrument field derotator is the first element in the optical train.

On-sky measurements of the optical distortion using IRDIS data from 47 Tucanae and NGC 3603 confirm that the SPHERE common path optical distortion dominates the telescope distortion effects. The SPHERE distortion at first order is an anamorphism of 0.60±0.02% between the horizontal and vertical pixel scales. This effect if uncorrected translates into an astrometric error of 6 mas at 1″, which is larger than the astrometric specifications for SPHERE (5 mas). Up to now, the consortium guaranteed-time data reduced at the SPHERE Data Center are corrected for this anamorphism (raw IRDIS images are vertically stretched by a factor 1.006), unlike for smaller higher-order distortion terms. The averaged error on the stellar positions over the full IRDIS field of view when neglecting higher-order distortion terms has been measured using 47 Tucanae data and estimated to be inferior to about 1 mas, i.e. inferior to 0.09 pixel.
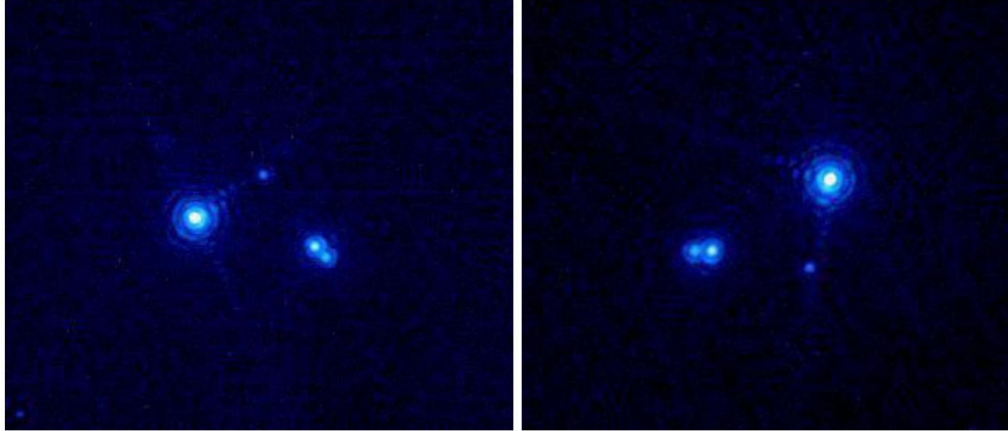
Figure 3. IRDIS images of the Trapezium B1–B4 in field-stabilized mode (left) and pupil-stabilized mode (right) for the same position angle of the SPHERE derotator.

3.2 ZEROPOINT ANGLE OF THE SPHERE PUPIL IN PUPIL-STABILIZED MODE

To align North up and East to the left, SPHERE images obtained in pupil-stabilized mode shall also be derotated from the zeropoint angle of the instrument pupil in this mode (Fig. 3). This parameter has been measured using commissioning and guaranteed-time data of several fields observed subsequently in field-stabilized mode and pupil-stabilized mode (with similar pointing parameters). The values measured between July 2014 and February 2016 were stable around an averaged value of $-136.03 \pm 0.13°$. After February 2016, we measured a change in the offset value and found an averaged value of $-135.44 \pm 0.09°$.

3.3 IRDIS

3.3.1 Pixel scale

The pixel scale of IRDIS has been measured at several epochs for various instrument setups (filter pair, coronagraph). The apodized pupil Lyot coronagraphs and four-quadrant phase masks of SPHERE[16] are made of material deposited on transparent substrates so that the pixel scale is expected to slightly change from one device to another. SPHERE includes also classical Lyot coronagraphs[16], for which the pixel scale is identical to the pixel scale measured without coronagraph (the opaque masks are suspended in this case). For given instrument setup and calibration field, measurements close in time are stable at a level of 0.009 mas/pixel. We show in the left panel of Fig. 4 individual pixel scale measurements for three fields observed with the H2 filter and the N_ALC_YJH_S apodized pupil Lyot coronagraph (diameter 185 mas), which is the coronagraph used for the consortium guaranteed-time survey. The error bars can vary between measurements on a given stellar cluster field according to the number of stars used for the analysis (differences in integration times, observing conditions, etc). Table 2 summarizes the current pixel scale estimates for all IRDIS filters for the N_ALC_YJH_S apodized pupil Lyot coronagraph. We considered 47 Tucanae as the reference field. For the filters with no available observations with 47 Tucanae, we accounted for pixel scale systematics between the observed field and 47 Tucanae by using pixel scale measurements from the two fields obtained with the H2 filter with coronagraph. The current estimate for the pixel scale for the H2 filter with the N_ALC_YJH_S coronagraph is 12.255 ± 0.009 mas/pix (specifications 12.25 ± 0.01 mas/pix). We note a decreasing trend for the pixel scale with the central wavelength of the filter up to the H band, followed by an increasing trend for longer wavelengths. When using no coronagraph, the pixel scale for a given filter is slightly decreased by a factor 1.0015. A calibration table with the pixel scale values for all IRDIS filter and coronagraph configurations is implemented to the SPHERE Data Center pipeline for the analysis of the consortium guaranteed-time data.

3.3.2 True North offset

The true North offset does not depend on the filter for a given observing run. Individual measurements of the true North offset over 2 years of SPHERE operations are listed in Tab. 3 and displayed in the right panel of

Table 2. On-sky measurements of the IRDIS pixel scale as a function of the filter.

Filter	Y2	Y3	J2	J3	H2	H3	K1	K2	BB_J	BB_H	BB_Ks
Scale (mas/pix)	12.283	12.283	12.266	12.261	12.255	12.250	12.267	12.263	12.263	12.251	12.265

Fig. 4. The most accurate measurements (with uncertainties below 0.05°) from July 2014 to late November 2015 show small variations of 0.15° with an average value of -1.70°. For a given stellar cluster, the error bars can vary from one observation to another because of the depth (integration time, use or not of a coronagraph) and the quality of the images. However, the true North measurements exhibit variations as large as 1° for the runs spanning from mid-December to late February, and the measurements obtained for the late March, mid-April, and late May runs are very stable within a same run, while small variations are present between the runs. The cause for these measurement variations is currently under investigation, including its link with the instrument's active support structure which shows some deviating behavior since late 2015. However, the amplitude of the latter effect is found to be an order of magnitude smaller than the observed true North deviation. Thus, this cause is ruled out.

Table 3. Individual measurements for the IRDIS true North as a function of the observing run.

Date	Field	True North (deg)
2014-07-18	47 Tuc	-1.762±0.043
2014-08-05	47 Tuc	-1.642±0.039
2014-10-11	47 Tuc	-1.781±0.042
2014-12-02	47 Tuc	-1.757±0.051
2015-02-03	Θ^1 Ori B	-1.73±0.06
2015-03-31	NGC 3603	-1.682±0.054
2015-05-03	HIP 67745	-1.81±0.15
2015-05-03	HIP 68725	-2.34±0.14
2015-05-30	NGC 6380	-1.693±0.063
2015-06-07	NGC 3603	-1.692±0.058
2015-06-28	NGC 6380	-1.767±0.055
2015-07-31	NGC 6380	-1.710±0.081
2015-09-24	47 Tuc	-1.631±0.046
2015-11-29	47 Tuc	-1.684±0.048
2015-12-20	Θ^1 Ori B	-1.85±0.29
2015-12-26	Θ^1 Ori B	-2.05±0.29

Date	Field	True North (deg)
2016-01-02	Θ^1 Ori B	-1.73±0.29
2016-01-16	Θ^1 Ori B	-2.25±0.42
2016-01-18	Θ^1 Ori B	-1.89±0.42
2016-01-20	Θ^1 Ori B	-2.27±0.42
2016-01-23	Θ^1 Ori B	-2.75±0.42
2016-02-07	Θ^1 Ori B	-1.77±0.42
2016-02-20	Θ^1 Ori B	-2.00±0.42
2016-03-26	Θ^1 Ori B	-1.81±0.07
2016-03-28	Θ^1 Ori B	-1.82±0.08
2016-03-30	NGC 3603	-1.653±0.061
2016-04-01	NGC 3603	-1.634±0.056
2016-04-16	NGC 3603	-1.519±0.059
2016-04-16	NGC 3603	-1.522±0.056
2016-05-22	NGC 3603	-1.648±0.080
2016-05-25	NGC 3603	-1.610±0.049

3.4 IFS

3.4.1 Pixel scale of the reconstructed data cubes

Due to the small field of view of IFS, direct on-sky astrometric calibration is currently feasible on the Orion Trapezium B1–B4 quadruple only (Fig. 5). The measurements give values of the pixel scale of 7.46±0.02 mas/pixel (specifications 7.4±0.1 mas/pix), which is the value used as default in the SPHERE Data Center pipeline. Nevertheless, since IFS can be operated only in parallel with IRDIS, indirect calibrations are derived using the on-sky IRDIS pixel scale and the IRDIS/IFS pixel scale ratio from IRDIS and IFS distortion grid data recorded simultaneously (Fig. 2).
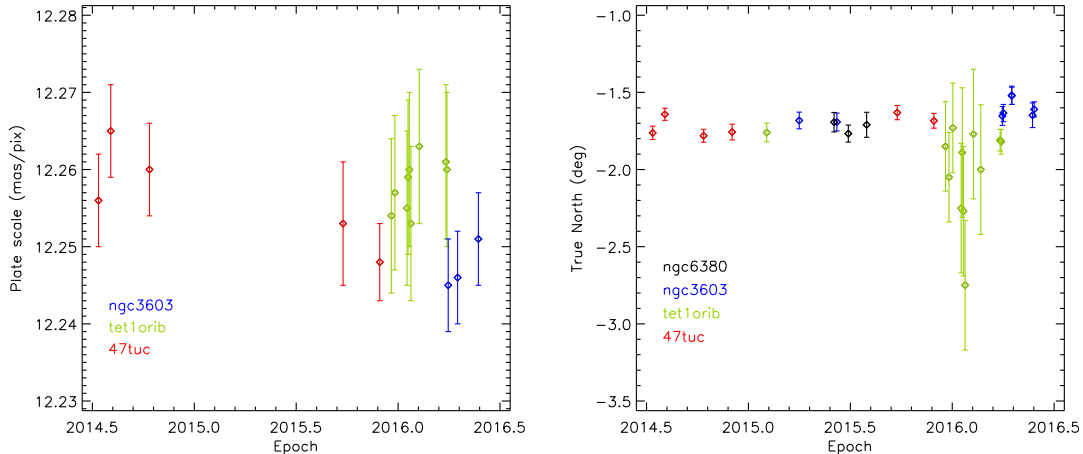
Figure 4. Individual measurements for the pixel scale (left) and true North (right) of IRDIS. For the pixel scale measurements, only the configuration H2 filter + N_ALC_YJH_S coronagraph is considered.
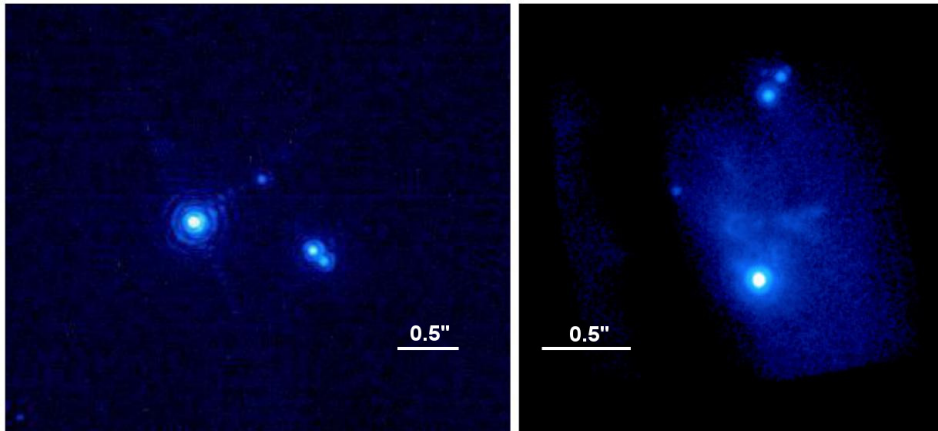

Figure 5. IRDIS (left) and IFS (right) images of the Orion Trapezium B1–B4 quadruple.

3.4.2 Angle offset between the IFS and IRDIS fields of view

Since IFS operates in parallel with IRDIS, the IRDIS true North measurement from any run (Tab. 3) is also applied to IFS images. An additional derotation is included to align the North up and the East to the left since the IFS field of view is rotated with respect to the IRDIS field of view (Fig. 5). The current estimate of this relative orientation is $+100.48\pm0.10°$. The on-sky estimate is consistent with the measurements obtained using internal calibration grids of the two instruments ($+100.55\pm0.10°$).

4. SUMMARY AND PROSPECTS

We have presented the current on-sky results for the astrometric calibration of the SPHERE near-infrared instruments (IRDIS and IFS) based on data collected over 2 years of operation. On-sky measurements of the SPHERE+VLT optical distortion show that the optical distortion from the VLT is negligible with respect to the SPHERE optical distortion and that the main SPHERE distortion effect results in a horizontal pixel scale $0.60\pm0.02\%$ larger than the vertical pixel scale for the IRDIS camera. Then, we estimated the zeropoint angle of the SPHERE pupil in pupil-stabilized mode, which is the main observing mode used for the consortium guaranteed-time exoplanet imaging survey. While we found that this parameter was stable around an averaged value of $-136.03\pm0.13°$ from July 2014 to February 2016, we observed since then a change of $+0.6°$ for this

parameter to an averaged value of $-135.44\pm0.09°$. We measured the pixel scale for IRDIS for various filter pairs and coronagraphs as well as the true North offset from July 2014 to May 2016. For given instrument configuration and astrometric calibration field, the pixel scale has a stability over a timescale of a few months of 0.009 mas/pixel. For coronagraphic data obtained with the H2 filter, our current estimate of the pixel scale is 12.255 ± 0.009 mas/pix. The statistics on the true North measurements from July 2014 to late November 2015 give a remarkable stable value of $-1.70\pm0.08°$. However due to a technical problem, the true North displayed variations up to $0.5°$ within a same run from mid-December 2015 to late February 2016. The origin of this anomalous instability is still under investigation. After a technical intervention on the instrument in March 2016, the stability of the true North measurements within a given run was much improved while small variations are still seen between the runs (some contribution from the astrometric field selection is also present). For the IFS reconstructed data cubes, on-sky and internal calibration data indicate an averaged pixel scale value of 7.46 ± 0.02 mas/pix and a relative orientation to the IRDIS field of view of $+100.48\pm0.10°$.

As part of the consortium guaranteed-time observations, we will continue to monitor the SPHERE astrometric parameters for the full survey. The public release of the GAIA data in late 2016 will provide absolute astrometric calibration for several of the SPHERE astrometric fields, which will help in improving the absolute calibration of the SPHERE data. We plan to release our consortium astrometric tool and observing procedures to ESO so that such analyses can also be carried out on a regular basis by the observatory. The results from these analyses will be made available to the SPHERE users outside the instrument consortium on a public web page.

Common astrometric fields observed with various high-contrast imaging instruments (e.g., SPHERE, GPI, LMIRCam, MagAO, CHARIS) will allow a better comparison of astrometric measurements from different instruments and a reduction of the systematic errors, which are a major issue for the determination of the orbital properties of directly-imaged companions in particular for those located at wide separations. We note that the Orion Trapezium field is very suitable to these comparisons because of its observability from both northern and southern hemispheres.

REFERENCES

1. C. Marois, B. Macintosh, T. Barman, B. Zuckerman, I. Song, J. Patience, D. Lafrenière, and R. Doyon, "Direct imaging of multiple planets orbiting the star hr 8799," *Science* **322**, pp. 1348–1352, nov 2008.

2. A.-M. Lagrange, M. Bonnefoy, G. Chauvin, D. Apai, D. Ehrenreich, A. Boccaletti, D. Gratadour, D. Rouan, D. Mouillet, S. Lacour, and M. Kasper, "A giant planet imaged in the disk of the young star β pictoris," *Science* **329**, pp. 57–59, 2010.

3. B. Macintosh, J. R. Graham, T. Barman, R. J. De Rosa, Q. Konopacky, M. S. Marley, C. Marois, E. L. Nielsen, L. Pueyo, A. Rajan, J. Rameau, D. Saumon, J. J. Wang, J. Patience, M. Ammons, P. Arriaga, E. Artigau, S. Beckwith, J. Brewster, S. Bruzzone, J. Bulger, B. Burningham, A. S. Burrows, C. Chen, E. Chiang, J. K. Chilcote, R. I. Dawson, R. Dong, R. Doyon, Z. H. Draper, G. Duchêne, T. M. Esposito,

D. Fabrycky, M. P. Fitzgerald, K. B. Follette, J. J. Fortney, B. Gerard, S. Goodsell, A. Z. Greenbaum, P. Hibon, S. Hinkley, T. H. Cotten, L.-W. Hung, P. Ingraham, M. Johnson-Groh, P. Kalas, D. Lafreniere, J. E. Larkin, J. Lee, M. Line, D. Long, J. Maire, F. Marchis, B. C. Matthews, C. E. Max, S. Metchev, M. A. Millar-Blanchaer, T. Mittal, C. V. Morley, K. M. Morzinski, R. Murray-Clay, R. Oppenheimer, D. W. Palmer, R. Patel, M. D. Perrin, L. A. Poyneer, R. R. Rafikov, F. T. Rantakyrö, E. L. Rice, P. Rojo, A. R. Rudy, J.-B. Ruffio, M. T. Ruiz, N. Sadakuni, L. Saddlemyer, M. Salama, D. Savransky, A. C. Schneider, A. Sivaramakrishnan, I. Song, R. Soummer, S. Thomas, G. Vasisht, J. K. Wallace, K. Ward-Duong, S. J. Wiktorowicz, S. G. Wolff, and B. Zuckerman, "Discovery and spectroscopy of the young jovian planet 51 Eri b with the Gemini Planet Imager," *Science* **350**, pp. 64–67, Oct. 2015.

4. M. R. Bate, "Stellar, brown dwarf and multiple star properties from hydrodynamical simulations of star cluster formation," *MNRAS* **392**, pp. 590–616, Jan. 2009.

5. D. Raghavan, H. A. McAlister, T. J. Henry, D. W. Latham, G. W. Marcy, B. D. Mason, D. R. Gies, R. J. White, and T. A. ten Brummelaar, "A Survey of Stellar Families: Multiplicity of Solar-type Stars," *ApJS* **190**, pp. 1–42, Sept. 2010.

6. L. M. Close, R. Lenzen, J. C. Guirado, E. L. Nielsen, E. E. Mamajek, W. Brandner, M. Hartung, C. Lidman, and B. Biller, "A dynamical calibration of the mass-luminosity relation at very low stellar masses and young ages," *Nature* **433**, pp. 286–289, Jan. 2005.

7. J. R. Crepp, J. A. Johnson, D. A. Fischer, A. W. Howard, G. W. Marcy, J. T. Wright, H. Isaacson, T. Boyajian, K. von Braun, L. A. Hillenbrand, S. Hinkley, J. M. Carpenter, and J. M. Brewer, "The Dynamical Mass and Three-dimensional Orbit of HR7672B: A Benchmark Brown Dwarf with High Eccentricity," *ApJ* **751**, p. 97, June 2012.

8. M. Bonnefoy, G.-D. Marleau, R. Galicher, H. Beust, A.-M. Lagrange, J.-L. Baudino, G. Chauvin, S. Borgniet, N. Meunier, J. Rameau, A. Boccaletti, A. Cumming, C. Helling, D. Homeier, F. Allard, and P. Delorme, "Physical and orbital properties of β Pictoris b," *A&A* **567**, p. L9, July 2014.

9. A. Burrows, M. Marley, W. B. Hubbard, J. I. Lunine, T. Guillot, D. Saumon, R. Freedman, D. Sudarsky, and C. Sharp, "A nongray theory of extrasolar giant planets and brown dwarfs," *ApJ* **491**, pp. 856–875, 1997.

10. I. Baraffe, G. Chabrier, T. S. Barman, F. Allard, and P. H. Hauschildt, "Evolutionary models for cool brown dwarfs and extrasolar giant planets. the case of hd 209458," *A&A* **402**, pp. 701–712, 2003.

11. F. Allard, D. Homeier, and B. Freytag, "Models of very-low-mass stars, brown dwarfs and exoplanets," *Royal Society of London Philosophical Transactions Series A* **370**, pp. 2765–2777, June 2012.

12. D. S. Spiegel and A. Burrows, "Spectral and Photometric Diagnostics of Giant Planet Formation Scenarios," *ApJ* **745**, p. 174, Feb. 2012.

13. J.-L. Beuzit, M. Feldt, K. Dohlen, D. Mouillet, P. Puget, F. Wildi, L. Abe, J. Antichi, A. Baruffolo, P. Baudoz, A. Boccaletti, M. Carbillet, J. Charton, R. Claudi, M. Downing, C. Fabron, P. Feautrier, E. Fedrigo, T. Fusco, J.-L. Gach, R. Gratton, T. Henning, N. Hubin, F. Joos, M. Kasper, M. Langlois, R. Lenzen, C. Moutou, A. Pavlov, C. Petit, J. Pragt, P. Rabou, F. Rigal, R. Roelfsema, G. Rousset, M. Saisse, H.-M. Schmid, E. Stadler, C. Thalmann, M. Turatto, S. Udry, F. Vakili, and R. Waters, "Sphere: a planet finder instrument for the vlt," in *SPIE Conf. Ser.*, I. S. McLean and M. M. Casali, eds., **7014**, p. 701418, 2008.

14. T. Fusco, J.-F. Sauvage, C. Petit, A. Costille, K. Dohlen, D. Mouillet, J.-L. Beuzit, M. Kasper, M. Suarez, C. Soenke, E. Fedrigo, M. Downing, P. Baudoz, A. Sevin, D. Perret, A. Barrufolo, B. Salasnich, P. Puget, F. Feautrier, S. Rochat, T. Moulin, A. Deboulbé, E. Hugot, A. Vigan, D. Mawet, J. Girard, and N. Hubin, "Final performance and lesson-learned of SAXO, the VLT-SPHERE extreme AO: from early design to on-sky results," in *SPIE Conf. Ser.*, **9148**, p. 91481U, Aug. 2014.

15. E. Hugot, M. Ferrari, K. El Hadi, A. Costille, K. Dohlen, P. Rabou, P. Puget, and J. L. Beuzit, "Active optics methods for exoplanet direct imaging. Stress polishing of supersmooth aspherics for VLT-SPHERE planet finder," *A&A* **538**, p. A139, Feb. 2012.

16. A. Boccaletti, L. Abe, J. Baudrand, J.-B. Daban, R. Douet, G. Guerri, S. Robbe-Dubois, P. Bendjoya, K. Dohlen, and D. Mawet, "Prototyping coronagraphs for exoplanet characterization with SPHERE," in *SPIE Conf. Ser.*, **7015**, p. 70151B, July 2008.

17. K. Dohlen, M. Langlois, M. Saisse, L. Hill, A. Origne, M. Jacquet, C. Fabron, J.-C. Blanc, M. Llored, M. Carle, C. Moutou, A. Vigan, A. Boccaletti, M. Carbillet, D. Mouillet, and J.-L. Beuzit, "The infra-red dual imaging and spectrograph for SPHERE: design and performance," in *SPIE Conf. Ser.*, **7014**, p. 70143L, Aug. 2008.

18. R. U. Claudi, M. Turatto, R. G. Gratton, J. Antichi, M. Bonavita, P. Bruno, E. Cascone, V. De Caprio, S. Desidera, E. Giro, D. Mesa, S. Scuderi, K. Dohlen, J. L. Beuzit, and P. Puget, "SPHERE IFS: the spectro differential imager of the VLT for exoplanets search," in *SPIE Conf. Ser.*, **7014**, p. 70143E, Aug. 2008.

19. C. Thalmann, H. M. Schmid, A. Boccaletti, D. Mouillet, K. Dohlen, R. Roelfsema, M. Carbillet, D. Gisler, J.-L. Beuzit, M. Feldt, R. Gratton, F. Joos, C. U. Keller, J. Kragt, II, J. H. Pragt, P. Puget, F. Rigal, F. Snik, R. Waters, and F. Wildi, "SPHERE ZIMPOL: overview and performance simulation," in *SPIE Conf. Ser.*, **7014**, p. 70143F, July 2008.

20. A. Vigan, C. Moutou, M. Langlois, F. Allard, A. Boccaletti, M. Carbillet, D. Mouillet, and I. Smith, "Photometric characterization of exoplanets using angular and spectral differential imaging," *MNRAS* **407**, pp. 71–82, 2010.

21. C. Marois, D. Lafrenière, R. Doyon, B. Macintosh, and D. Nadeau, "Angular differential imaging: A powerful high-contrast imaging technique," *ApJ* **641**, pp. 556–564, apr 2006a.

22. C. Marois, D. W. Phillion, and B. Macintosh, "Exoplanet detection with simultaneous spectral differential imaging: effects of out-of-pupil-plane optical aberrations," in *SPIE Conf. Ser.*, *Proc. of SPIE* **6269**, p. 62693M, jul 2006.

23. A. Sivaramakrishnan and B. R. Oppenheimer, "Astrometry and Photometry with Coronagraphs," *ApJ* **647**, pp. 620–629, Aug. 2006.

24. M. Langlois, A. Vigan, C. Moutou, J.-F. Sauvage, K. Dohlen, A. Costille, D. Mouillet, and D. Le Mignant, "Infrared Differential Imager and Spectrograph for SPHERE: Performance Status with Extreme Adaptive Optics before shipment to ESO/VLT," in *Proceedings of the Third AO4ELT Conference*, S. Esposito and L. Fini, eds., p. 63, Dec. 2013.

25. R. Racine, G. A. H. Walker, D. Nadeau, R. Doyon, and C. Marois, "Speckle Noise and the Detection of Faint Companions," *PASP* **111**, pp. 587–594, May 1999.

26. W. B. Sparks and H. C. Ford, "Imaging spectroscopy for extrasolar planet detection," *ApJ* **578**, pp. 543–564, 2002.

27. A. Zurlo, A. Vigan, D. Mesa, R. Gratton, C. Moutou, M. Langlois, R. U. Claudi, L. Pueyo, A. Boccaletti, A. Baruffolo, J.-L. Beuzit, A. Costille, S. Desidera, K. Dohlen, M. Feldt, T. Fusco, T. Henning, M. Kasper, P. Martinez, O. Moeller-Nilsson, D. Mouillet, A. Pavlov, P. Puget, J.-F. Sauvage, M. Turatto, S. Udry, F. Vakili, R. Waters, and R. F. Wildi, "Performance of the VLT Planet Finder SPHERE. I. Photometry and astrometry precision with IRDIS and IFS in laboratory," *A&A* **572**, p. A85, Dec. 2014.

28. S. Trippe, S. Gillessen, O. E. Gerhard, H. Bartko, T. K. Fritz, H. L. Maness, F. Eisenhauer, F. Martins, T. Ott, K. Dodds-Eden, and R. Genzel, "Kinematics of the old stellar population at the Galactic centre," *A&A* **492**, pp. 419–439, Dec. 2008.

29. L. M. Close, A. Puglisi, J. R. Males, C. Arcidiacono, A. Skemer, J. C. Guerra, L. Busoni, G. Brusa, E. Pinna, D. L. Miller, A. Riccardi, D. W. McCarthy, M. Xompero, C. Kulesa, F. Quiros-Pacheco, J. Argomedo, J. Brynnel, S. Esposito, F. Mannucci, K. Boutsia, L. Fini, D. J. Thompson, J. M. Hill, C. E. Woodward, R. Briguglio, T. J. Rodigas, R. Briguglio, P. Stefanini, G. Agapito, P. Hinz, K. Follette, and R. Green, "High-resolution Images of Orbital Motion in the Orion Trapezium Cluster with the LBT AO System," *ApJ* **749**, p. 180, Apr. 2012.

30. Z. Khorrami, T. Lanz, F. Vakili, E. Lagadec, M. Langlois, W. Brandner, O. Chesneau, M. R. Meyer, M. Carbillet, L. Abe, D. Mouillet, J. L. Beuzit, A. Boccaletti, C. Perrot, C. Thalmann, H.-M. Schmid, A. Pavlov, A. Costille, K. Dohlen, D. Le Mignant, C. Petit, and J. F. Sauvage, "VLT/SPHERE deep insight of NGC 3603's core: Segregation or confusion?," *A&A* **588**, p. L7, Apr. 2016.

31. A. Bellini, J. Anderson, R. P. van der Marel, L. L. Watkins, I. R. King, P. Bianchini, J. Chanamé, R. Chandar, A. M. Cool, F. R. Ferraro, H. Ford, and D. Massari, "Hubble Space Telescope Proper Motion (HST-PROMO) Catalogs of Galactic Globular Clusters. I. Sample Selection, Data Reduction, and NGC 7078 Results," *ApJ* **797**, p. 115, Dec. 2014.

32. A. Pavlov, O. Möller-Nilsson, M. Feldt, T. Henning, J.-L. Beuzit, and D. Mouillet, "SPHERE data reduction and handling system: overview, project status, and development," in *SPIE Conf. Ser.*, **7019**, p. 701939, July 2008.

33. C. B. Markwardt, "Non-linear Least-squares Fitting in IDL with MPFIT," in *Astronomical Data Analysis Software and Systems XVIII*, D. A. Bohlender, D. Durand, and P. Dowler, eds., *ASP Conf. Ser.* **411**, p. 251, Sept. 2009.

34. F. Wildi, D. Mouillet, J.-L. Beuzit, M. Feldt, K. Dohlen, T. Fusco, C. Petit, S. Desidera, R. Gratton, H.-M. Schmid, M. Langlois, A. Vigan, J. Charton, R. Claudi, R. Roelfsema, A. Baruffolo, and P. Puget, "Calibrating SPHERE, the exo-planet imager for the VLT," in *Techniques and Instrumentation for Detection of Exoplanets IV*, *Proc. SPIE* **7440**, p. 74400Q, Aug. 2009.